

Effective affinities in microarray data

T. Heim

Interdisciplinary Research Institute c/o IEMN, Cité Scientifique BP 60069, F-59652 Villeneuve d'Ascq, France

J. Klein Wolterink

Institute for Theoretical Physics, University of Utrecht, Leuvenlaan 4, 3584 CE Utrecht

E. Carlon

Interdisciplinary Research Institute c/o IEMN, Cité Scientifique BP 60069, F-59652 Villeneuve d'Ascq, France and
Ecole Polytechnique Universitaire de Lille, Cité Scientifique, F-59655 Villeneuve d'Ascq, France

G. T. Barkema

Institute for Theoretical Physics, University of Utrecht, Leuvenlaan 4, 3584 CE Utrecht

(dated: September 5, 2021)

In the past couple of years several studies have shown that hybridization in Affymetrix DNA microarrays can be rather well understood on the basis of simple models of physical chemistry. In the majority of the cases a Langmuir isotherm was used to fit experimental data. Although there is a general consensus about this approach, some discrepancies between different studies are evident. For instance, some authors have fitted the hybridization affinities from the microarray fluorescent intensities, while others used affinities obtained from melting experiments in solution. The former approach yields affinities that at first sight are only partially consistent with solution values. In this paper we show that this discrepancy exists only superficially: a sufficiently complete model provides effective affinities which are fully consistent with those fitted to experimental data. This link provides new insight on the relevant processes underlying the functioning of DNA microarrays.

PACS numbers: 87.15.-v, 82.39.Pj

I. INTRODUCTION

In all living cells the genes are transcribed, *i.e.*, copied into messenger RNA (mRNA), at different rates [1]. These rates depend on the type of cell, on the stage of the cell life cycle and on other external stimuli, like changes of pH, temperature or on the presence of chemicals. The abundance of a specific mRNA defines the so-called gene expression level. It is of central importance to understand when, in which tissue and in which amount a given gene is expressed. This knowledge is for instance crucial in understanding several diseases that originate from deregulations in the gene transcription process, *i.e.*, those pathologies triggered by genes which are overexpressed or underexpressed.

DNA microarrays have become pivotal devices in molecular biology as they allow a genome-wide screening of gene expression levels in a single experiment. Both commercial and homemade microarrays are nowadays available. One of the leading companies in the DNA-microarray market is Affymetrix, which produces high-density oligonucleotide microarrays [2]. In Affymetrix arrays, photolithographic techniques are used to grow on a solid substrate single-stranded DNA sequences which are 25 nucleotides long; these are normally referred to as probes. The array is placed in contact with a solution containing RNA molecules, *i.e.*, the targets, extracted from biological samples. Those targets that are complementary to probe sequences tend to bind to these, a process known as hybridization. Biotin molecules are attached to

a fraction of the nucleotides in the target sequences. Once hybridization has occurred and the unbound targets are washed away, streptavidin molecules, which carry fluorescent labels, are added to the solution. The latter bind with high affinity to the biotin so that the amount of hybridized probe-target duplexes can be determined experimentally by optical measurements.

Two specific aspects of Affymetrix arrays are: 1) Several probes are complementary to the same target molecule (these probes form the so-called probe set) and 2) Each perfect matching (PM) probe has a partner probe which differs by a single nucleotide in the middle position, the so-called mismatch (MM) probe. The use of multiple probes for the same target RNA increases the reliability of the determination of gene expression levels in Affymetrix arrays, which are obtained from simultaneous measurements of several fluorescent signals. The signals measured from MM probes can be used as test for the quality of the hybridization experiment. Usually, one expects that PM probes give a stronger signal than the corresponding MM probes. However, "bright mismatches", *i.e.*, higher signals from MM than PM probes, are observed quite frequently [3].

The hybridization of complementary strands in solution, or the reverse process of DNA/RNA melting, has been widely investigated in the past years [4]. Measurements of melting temperatures of short oligonucleotides have yielded estimates of the enthalpy and entropy differences H and S between a double helix and the two separate strands. It turns out that H and S

TABLE I: The stacking free energy parameters G for RNA/DNA hybrids measured in solution at a salt concentration of 1 M NaCl and at 45 °C [5]. The upper strand is RNA (with orientation 5'-3') and lower strand DNA (orientation 3'-5'). The helix initiation energy is $G^{\text{init}} = 3.14$ kcal/mole.

Sequence	G (kcal/mole)	Sequence	G (kcal/mole)
rA A dT T	0.83	rA C dT G	1.99
rA G dT C	1.62	rA U dT A	0.70
rC A dG T	0.70	rC C dG G	1.92
rC G dG C	1.32	rC U dG A	0.73
rG A dC T	1.21	rG C dC G	2.56
rG G dC C	2.65	rG U dC A	0.93
rU A dA T	0.42	rU C dA G	1.31
rU G dA C	1.37	rU U dA A	-0.08

can be well approximated by a sum over local terms depending on pairs of neighboring nucleotides, plus eventual boundary terms. This defines the so-called nearest-neighbor model [4]. Table I gives an example of nearest-neighbor free energy parameters obtained from measurements of melting temperatures of DNA/RNA duplexes in solution. The free energy differences are obtained from $G = H - TS$, assuming that the experimentally measured H and S are temperature independent.

The hybridization process in microarrays is not identical to that in solution, as one of the two strands is surface-bound. A review of recent work on the hybridization on surface immobilized DNA [6] shows that the rate constants for hybridization are lower than those predicted by the nearest neighbor model in solution. The comparison was done with experiments with a single species target and probes of equal length [7, 8, 9].

Several studies [3, 10, 11, 12, 13, 14, 15] recently discussed the role of the Langmuir isotherm and variants thereof in connection with DNA microarrays. Research toward a physics-based modeling of hybridization in Affymetrix arrays can roughly be divided into two approaches. The first approach is to identify empirical functions with many degrees of freedom, that are fitted to experimental data [3, 16]. The other approach is molecular-based and employs the hybridization energies in solution; it then requires a rescaling of parameters like the effective temperature [12, 17]. The aim of this paper is to link these two apparently different viewpoints. We shall show indeed that, when the appropriate quantities

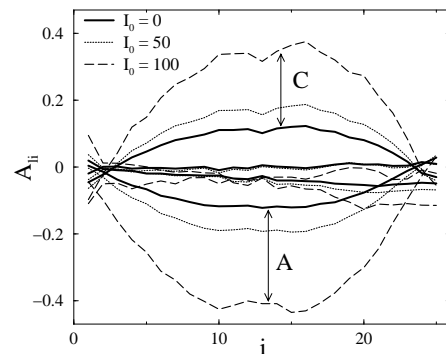


FIG. 1: Position-dependent effective affinities fitted from Affymetrix data of the HG U95A chipset. Three different background values are subtracted: $I_0 = 0, 50$ and 100 . The three topmost curves are the affinities for nucleotides C and the three lowest curves for the nucleotides A. The affinities for T and G are almost degenerate.

are compared, i.e. the effective affinities, the two models yield fully consistent results.

This paper is organized as follows: Sec. II reanalyzes the binding affinities as introduced by Naef and Magnasco [3] and Binder and Preibisch [16]. We carry out a sensitivity analysis and show which features are robust and which are sensitive. In Sec. III, effective affinities are calculated using a molecular model based on the binding free energies of Sugimoto et al. [5] and the extension by Carbon and Heim [17]. From this model, the influence of different additions to the molecular model on the effective affinities is calculated and analyzed. Section IV concludes the paper and summarizes the main results.

II. EFFECTIVE AFFINITIES FOR AFFYMETRIX ARRAYS

We turn now to the determination of the effective affinities from the analysis of Affymetrix data. We follow here and further the procedure originally introduced by Naef and Magnasco [3] and extended more recently by Binder and Preibisch [16].

Naef and Magnasco treat the brightness B of perfect-matching probes as a function of their sequence composition:

$$\ln \frac{B}{[RNA]} = \sum_{li} S_{li} A_{li}; \quad (1)$$

where $l = A; C; G; T$ is the letter index and $i = 1; \dots; 25$ the position along the probe. S_{li} is a boolean variable equal to 1 if the probe sequence has letter l at position i and 0 otherwise, and thus A_{li} are per-site, per-letter affinities. The median of the PM brightnesses $[RNA]$ is used in this expression as a surrogate for the RNA concentration, which is not known for most Affymetrix data.

In Affymetrix experiments, the brightness B will saturate, once the majority of the probes are bound to targets. Capturing such saturation requires the use of Langmuir isotherms; the approach above (eq. (1)) neglects saturation effects, and hence is only expected to work in the so-called Henry regime [18] signified by brightnesses much lower than the maximal value. Since only few probes reach saturation, neglecting saturation is justifiable.

The experimentally measured fluorescence intensity I_s of a probe with sequence s does not approach zero at zero concentration of the matching target: there is a background signal, probably due to non-specific binding. To take this into consideration, we distinguish two contributions to the fluorescence intensity: a constant background intensity I_0 and the brightness B due to specific binding:

$$I_s = I_0 + B; \quad (2)$$

in which B is the brightness as in eq. (1). We tried different background subtraction schemes in order to test the robustness of the data. Fig. 1 shows the position-dependent affinities A_{ii} obtained from fitting the experimental data to eqs. (1) and (2) for background intensities of $I_0 = 0, 50$ and 100 (constant background level). In the plot, the distance of the data to the model was minimized in the logarithmic scale. We note that although the shape of the fitted position-dependent affinities remain the same in the three cases, the amplitudes vary by a factor of 4. In all cases the shape is consistent with what was found in Refs. [3, 16]: the position-dependent affinities are approximately symmetrical with respect to the central position of the probe ($i = 13$) and the highest affinity is for nucleotides C and the lowest for A in the probe sequence. The affinities for the G and T bases are almost degenerate and show less position dependence than the affinities for the C and A bases.

In the case of $I_0 = 0$ we have a rather low signal. This is somehow expected as in that case the non-specific part of the signal may dominate, which induces a loss of specificity. When higher values of I_0 are taken, a non-trivial signal starts to emerge. As I_0 increases, the amplitude of the strongest effective affinity increases to 0.2 and 0.4 for respectively $I_0 = 50$ and 100 .

In Fig. 2 we plot the fitted affinities A_{ii} for probe sets with an average intensity above 500. This case corresponds to signals well above the background level and thus the results should be weakly dependent of the value of I_0 chosen, as is indeed the case.

As mentioned above, using the median of the PM brightnesses [RNA] as an estimate for the RNA concentration is the only thing one can do in the absence of knowledge of its true value. Affymetrix, however, performed a set of experiments in which some target sequences are added in solution (spiked-in) at a known concentration. The results, known as the Latin square data set, are publicly available from the Affymetrix web site [19]. We used these data to re-fit the effective affinity

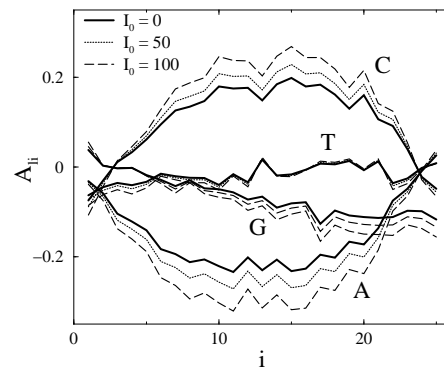


FIG. 2: As in Fig. 1, but disregarding all the data for probe sets with an average intensity below $I = 500$. The effective affinities are less sensitive to the choice of I_0 , compared with the fits of Fig. 1.

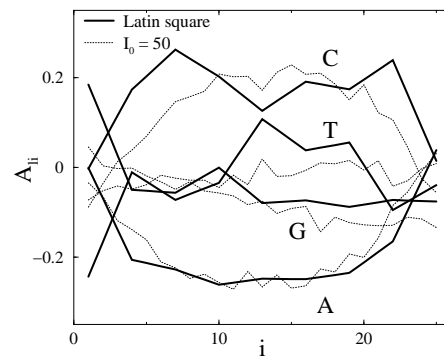


FIG. 3: Fit of Spike-in data of the HG U95A microarray using eq. (1). Here, we subtract from the intensity the known background intensity at zero concentration.

ties from eq. (1), using the true target concentration c_s of sequence s , rather than the median of the intensities. Due to the large number of parameters, this procedure yields typically values of A_{ii} that are too noisy. To limit the number of fitting parameters we therefore have fitted A_{ii} only at some fixed positions $i = 1; 4; 7; 10 :: 25$ and taken for the other values of i a linear interpolation between the two fitted numbers. Note that the Latin square set also contains a series of reference intensities measured in absence of the transcripts in solution (i.e. $c_s = 0$), a procedure that yields a direct estimate of the background signal I_0 . The position-dependent affinities obtained from the fitting of the Latin square set are shown in Fig. 3. The results, although still somewhat noisy, follow the general trend already shown in Figs. 1 and 2.

The fact that the position-dependent affinities are lower for G than for C and for A than for T is consistent with the hybridization data in solution, as pointed out in Ref. [20]. This apparent "asymmetry" is due to the asymmetry between DNA strands of the surface-bound probes and the RNA strands of the target molecules in

solution.

The fact that the effective affinities for G and T are close is quite surprising, given the clear differences in binding free energies in solution; we will argue below that this is due to hybridization between RNA target molecules in solution.

III. EFFECTIVE AFFINITIES RESULTING FROM MOLECULAR-BASED MODELS

To obtain more insight into the relation between the hybridization free energies of Table I and the effective affinities of Refs. [3, 16] and which we analyzed in the previous section, we extract effective affinities from a model which was recently proposed by two of us [17].

This model is based on ideas from Held et al. [12]. As it uses as input the binding free energies between DNA and RNA strands in solution reported in Table I, we will refer to it as the molecular-based model. Additionally, it incorporates the effect of binding in solution of RNA to RNA in an approximate way, tied to the intensities measured on an Affymetrix chip. The intensity I_s of sequence s is assumed to be proportional to the fraction of hybridized probes at the surface, described by a Langmuir model. In detail, it is given by [17]

$$I_s = I_0 + \frac{c_s Z_s}{1 + c_s Z_s} I_{\max}; \quad (3)$$

where c_s is the total concentration of targets with sequence s in solution, Z_s is the partition sum over states in which target s is bound to the probe, and c_s is the fraction of targets in solution which are free, and not hybridized in solution.

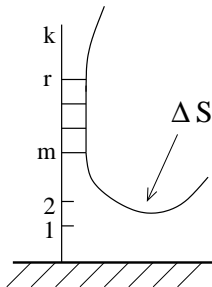


FIG. 4: Schematic picture of a partially hybridized configuration. The total probe length is k base pairs and we allow for $k < 25$, as the photolithographic process used by Affymetrix produces probes which are polydisperse. The target here is bound partially from bases m to bases r . We include in the calculation the entropy loss $S(m)$ due to the proximity of the target tail and the surface.

In the model of Ref. [17]

$$Z_s = \exp(-G_s); \quad (4)$$

where $\beta = 1/(RT)$ is the inverse temperature, and G_s is the total binding free energy for a perfectly formed helix of 25 base pairs between the RNA target and DNA probe. This binding free energy is described by

$$G_s = \sum_{i=1}^{24} S_{1,i} S_{i+1} G(l; l^0) + G^{\text{init}}; \quad (5)$$

As before, $S_{1,i}$ is a boolean variable equal to 1 if the probe sequence has letter l at position i and 0 otherwise. Thus, the sum in eq. (5) runs over all 24 stacking parameters $G(l; l^0)$, which depend on the identity of two neighboring nucleotides l and l^0 in the surface-bound DNA strand. G^{init} represents a helix initiation cost [4]. For the stacking parameters the model uses RNA/DNA free energies given in Table I, as obtained from experiments in solution [5]. Note that, differently from the approach of Refs. [3] and [16], the free energies used here are position-independent. In Ref. [17], the inverse temperature in eq. (4) is taken as a fitting parameter.

We stress that in Ref. [17] the hybridization free energy $G = H - TS$ was taken at $T = 37^\circ\text{C}$, while an Affymetrix hybridization experiment is performed at $T = 45^\circ\text{C}$, which is the value we consider here (see Table I). Although the temperature differs by only 8°C , the G 's on average differ by about 20%, since H and TS are rather close. We took the sequences of the Latin square set (25 nucleotides of length) and generated G of each sequence at both temperatures. A plot of G_{37} vs. G_{45} shows that the values are narrowly distributed along a straight line. This implies that a difference between the two choices of parameters can be reabsorbed in a rescaling of β in eq. (4).

Of practical interest is the total concentration c_s of targets with sequence s . Due to hybridization of single-stranded RNA in the solution, the concentration of free targets, which can bind to the probes, is lower than the total concentration of targets in solution. In the model of Ref. [17], this is taken into account by reducing the total concentration c_s in solution by a factor of s given by

$$s = \frac{1}{1 + c_0 \exp(-\beta G_R)}; \quad (6)$$

where β^0 and c_0 are fitting parameters and G_R is the (sequence dependent) RNA/RNA binding free energy for duplex formation in solution, taken from Ref. [4]. Note that also s is highly sequence-dependent: CG-rich targets will have high affinity to the complementary surface bound probes, but will also have a strong tendency to hybridize in solution. It has been shown that a unique choice (i.e. probe-independent) of the parameters I_{\max} , β^0 and c_0 fits the experimental data well [17].

There are many similarities, and also some discrepancies, between the intensities I_s in the Naef and Magasco (NM) approach eq. (2) and in the molecular-based model eq. (3). The binding free energy in the NM approach is captured in the summation on the right-hand-side of

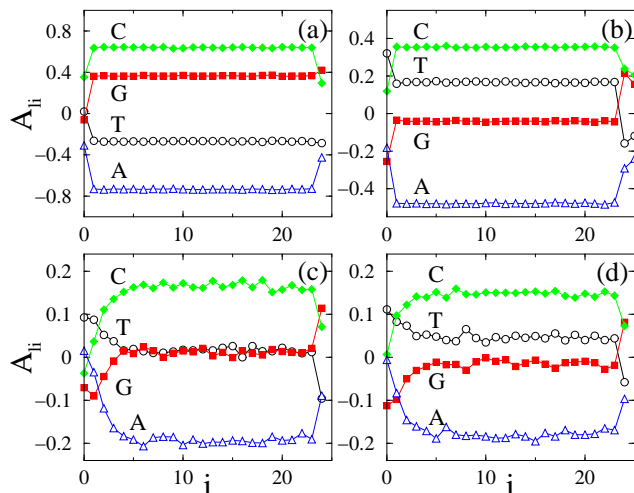


FIG. 5: Effective affinities, obtained with the molecular-based model, versus position in the probe, for the four different nucleotides. In panel (a) only the binding energy is taken into account; the effective temperature T is 800 K. In Figure (b), the hybridization in solution is also taken into account, as in the molecular-based model of Ref. [17]; the resulting effective temperature becomes $T = 570$ K. The effect of using the "zipper" and the probe length distribution is shown in Figure (c), resulting in an effective temperature of $T = 525$ K. In Figure (d) all effects mentioned in the text are taken into account and the effective temperature is reduced to $T = 494$ K.

eq. (1), which is very similar to the summation in eq. (5) in the molecular-based model. NM uses a summation over single base pairs with position-dependent affinities, while the molecular-based model uses (in eq. (5)) a summation over pairs of base pairs (allowing for stacking energies), with a position-independent strength. As we already mentioned, NM does not feature saturation, while the molecular-based model does through the denominator in eq. (3). Finally, the clear position-dependence in the effective affinities obtained with the NM approach is not included in the molecular-based model of Ref. [17].

A. Extending the molecular-based model

In this work, we introduce several extensions to the latter model. These extensions will cause position-dependence in the effective affinities, without ad-hoc modifications to the stacking free energy parameters. Most of these extensions are related to the fact that both target and probe are polydisperse in length, and that the duplex can fluctuate and partially unzip. We will first explain these extensions, and then discuss their effect later.

Unzipping. Besides the conformation in which the target is bound to the probe over its full length, other conformations occur in which the target covers only part of the probe. This is taken into ac-

count by a "zipper"-model. As a result, the partition sum Z_s does not only contain a single term $\exp(-G_s)$, but is a summation over many terms, each of which given by eq. (5), but in which the index i runs from the first bound pair m to the last bound pair $r - m$. This idea is visualized in Figure 4.

Probe length dispersity. During the production process of the Affymetrix chips, the probability p_g that the probe grows by an extra nucleotide is only around $p_g \approx 90\%$ [21]. This means that the fraction of probes which reach the final full length of 25 nucleotides is $P(25) = (p_g)^{25}$. The fraction of incomplete probes reaching a length $l < 25$ equals $P(l) = (p_g)^l (1 - p_g)$. We have included the effect of probe length dispersity by including these probabilities in the calculation. The intensity is therefore equal to $I = \sum_{l=1}^{25} P(l) I_l$, where I_l is the Langmuir isotherm corresponding to a probe of length l .

Non-specific binding. Even in Affymetrix experiments where no perfect matching targets are present, the intensity does not fall well below 0.5% of the maximal intensity. We attribute this to non-specific binding to the probes. To account for the non-specific binding, we include in our model a constant sequence-independent background intensity I_0 .

Tail repulsion. The RNA-target molecules often extend beyond the 25 base pairs of the probe; the average target length is 50 base pairs. The tail of the target which sticks out from the base of the probe is hindered significantly by the surface (see Figure 4). This causes an entropic repulsion between the target and the surface, lowering the intensity. The mathematics of this effect is presented in Appendix A. This effect is not sequence-dependent and the parameters Z_s in eq. (3) can therefore be multiplied by a constant factor $Z_{s, \text{tail}}$, given in eq. (A 4).

Fluorescent labels. Due to the fact that in the experiments only the U and C nucleotides can have a label, the fluorescence intensity will scale linearly with the number of U and C nucleotides, which obviously depends on the sequence. We therefore multiplied each Langmuir isotherm by for a factor $2X_{UC}$, in which X_{UC} is the fraction of U and C in the target sequence. We assumed that the target is simply composed of 25-mers.

B. Results of the model calculations

We generated 100,000 different random sequences of 25 nucleotides each. For each sequence $s = 1 \dots 10^5$, we also selected a concentration c_s , with a minimal value

of $c_{m_in} = 1$ picomolar and $c_{m_ax} = 1$ nanomolar (the typical range of target concentrations in Arrayex arrays); the logarithm of these concentrations $\log(c_s)$ is drawn from a uniform distribution $[\log(c_{m_in}); \log(c_{m_ax})]$. For each sequence s , the intensity I_s is calculated using the molecular-based model, eq. (3), with the extension just described. The parameters entering this equation are the stacking free energies given in Table I, as well as the parameter β_s reflecting the reduction of the total concentration of free targets in solution; this latter (sequence-dependent) parameter uses the RNA/RNA binding free energies for duplex formation in solution, taken from Ref. [4]. The modifications in the molecular-based model as compared to the model in Ref. [17], as well as the different choice of free energy parameters (G_{45} vs G_{37}) require a re-tuning of the effective inverse temperature β_0 and a concentration c_0 , which yielded $\beta_0 = 0.6$ (kcal/mole) $^{-1}$ and $c_0 = e^{-\beta_0}$, with $\beta_0 = 42$ kcal/mole. The tuning procedure for these two parameters follows the procedure of [17].

In the experimental Arrayex data set, the average intensity is around 3% of the maximal intensity. In all our simulations, we adjusted the temperature to reproduce this average intensity. The resulting temperatures range from 494 K to 550 K. There is still a gap between the experimental temperature of 318 K, but including the effects mentioned above has significantly decreased this gap in the original molecular-based model, where the effective temperature was 700 K [17]; in turn the latter model had already a much more realistic effective temperature than the Held model where the effective temperature exceeded 2000 K [12]. To obtain the effective affinities A_{ii} associated to the molecular-based model, we minimize the difference between the intensity I_s as predicted by the molecular model in eq. (3) and the intensity I_e resulting from the effective affinities and given by

$$\ln(I_e) = \sum_{ii} S_{ii} A_{ii} \ln(c_s); \quad (7)$$

in analogy to eq. (1). More precisely, the effective affinities A_{ii} result from a minimization of the sum over all 100,000 sequences of the squared difference between the logarithm of the intensity I_s and the logarithm of the intensity I_e resulting from the effective affinities.

The first data set comprises a simple two-state model, in which a target is either free in solution, or fully bound to a probe. Hybridization in solution is not taken into account, i.e., $\beta_s = 1$. The results are shown in Figure 5(a). The effective affinities do not depend on the position, apart from the two edge nucleotides which enter in only one pair of neighboring base pairs. (See eq. (5)). Note that the affinities increase with the ordering $A < T < G < C$, as expected from the values of the free energies of Table I.

Next, the hybridization in solution is taken into account by using two extra parameters β_0 and c_0 which have the values of $\beta_0 = 0.6$ (kcal/mole) $^{-1}$ and $c_0 = e^{-\beta_0}$ with $\beta_0 = 42$ kcal/mole, respectively. Still the effective affinities

are not position dependent, see Figure 5(b). However, the order of the curves has changed: $A < G < T < C$.

Fig. 5(c) shows the effective affinities when polydispersity of the probe length distribution and the effect that a duplex can zip open has been taken into account. These two effects lead to position-dependent effective affinities. The effect on the side of the microarray surface is larger than that on the solution side. Furthermore, the effective affinities of G and T have become more alike.

The last panel of Figure 5 shows the effective affinities when also the effect of noise, entropy of the tails, and the fact that only U and C carry fluorescent labels are taken into account. The biggest effect is that the effective temperature is lowered. Furthermore, the sequence has become $A < G < T < C$, in agreement with the order of effective affinities observed in experiment (see Figure. 2). Note also that the scale of amplitudes of the effective affinities ranges from about 0.2 to 0.2 (see Fig. 5(c-d)). This is fully consistent with the values obtained in Section II.

IV. CONCLUSIONS

In this paper we have analyzed the relation between the effective affinities as originally introduced by Naef and Magasco [3] and those obtained from a molecular-based model [17], which uses hybridization free energies in solution. We show that these two models yield very similar effective affinities. This implies that free energies in solution are adequate parameters to describe hybridization in Arrayex microarrays, at least if an effective temperature is used.

Firstly, the fact that the effective affinity for G is lower than that for C and that the affinity for A is lower than that for T is consistent with hybridization data in solution, as pointed out in Refs. [16, 20]. Here, we have shown the role of target-target hybridization in solution, which in the molecular-based approach [17] is described by a parameter β_s (see eq. (6)). The effect of β_s is of diminishing the differences in the effective affinities between different nucleotides so to make the effective affinities for G and T almost "degenerate" (see Fig. 5). This is consistent with the data of Naef and Magasco [3], Binder and Preibisch [16] and our results of Sec. II. The basic physics behind this effect is quite clear. The small difference between the effective affinities for G and T, in spite of the large difference in binding free energies in solution between these two nucleotides, is caused by the fact that G-rich sequences tend to hybridize strongly in solution, thereby diminishing their concentration available for binding to the probes.

We note that the calculation of the previous section yield effective affinities which are position-dependent, mostly caused by the ability of the probe-target complex to partly open up at the ends. To a lesser extent, also the target-surface repulsion and the polydispersity of the probes play a role. The profiles of the effective affinities

calculated in Sec. II are somewhat smoother than those deduced from the molecular-based model. This difference is however small. The most important aspect of our analysis is however that the molecular-based model 1) reproduces the degeneracy between the activities of G and T 2) yield amplitudes for the activities quantitatively close to those calculated in Sec. II.

We finally comment on other possible ways of linking effective activities to hybridization free energies obtained from melting experiments in solution. A recent study Ref. [22] attributed the differences between the two quantities to the effect of biotin molecules on the binding. This is an alternative point of view compared to our approach which emphasizes instead the effect of hybridization in solution between partially complementary single stranded RNA molecules. In this respect it would be interesting if measurements of melting temperatures experiments of biotinilated RNA and DNA duplexes in solution similar to that of Ref. [5] could be performed. These experiments would allow to quantify the effect of biotin on binding. To our knowledge such experiments have not yet been performed.

Acknowledgments

We acknowledge financial support from the Van Gogh Programme d'Actions Intégrées (PAI) 08505PB of the French Ministry of Foreign Affairs and NWO grant 62403735.

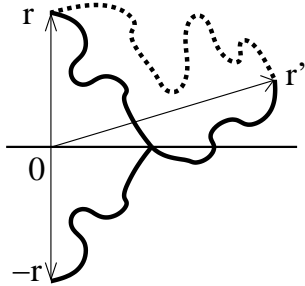


FIG. 6: The fraction of paths originating in $\mathbf{r} = (0;0;z)$ and never crossing the plane $z = 0$ can be found with the method of images: the number of paths crossing the plane and ending in \mathbf{r}^0 is equal to the total number of paths starting from \mathbf{r} and ending in \mathbf{r}^0 .

APPENDIX A: ENTROPIC REPULSION BETWEEN SUBSTRATE AND TARGET TAIL

We model the single-stranded DNA segment as a freely jointed chain with Kuhn length b . The probability dis-

tribution that a segment of N Kuhn steps extends to a distance \mathbf{r} from its origin is given by a Gaussian distribution:

$$P(\mathbf{r};N) = \frac{3}{2N b^2} e^{-3\mathbf{r}^2/2N b^2}; \quad (\text{A1})$$

To determine the number of polymers starting from a height z above the surface and not crossing the wall, we use the method of mirror images. Using the same conformation as in Figure 6: the fraction of walks of length N originating from $\mathbf{r} = (0;0;z)$ and terminating at $\mathbf{r}^0 = (0;0;z^0)$ is equal to $P(\mathbf{r}^0;N)$. A part of these cross the wall. This fraction is equal to $P(\mathbf{r}^0 + \mathbf{r};N)$, i.e. the number of walks originating in \mathbf{r} and terminating in \mathbf{r}^0 . Therefore the fraction of walks of total length N starting in \mathbf{r} and terminating in \mathbf{r}^0 and which do not cross the wall is given by the difference:

$$\begin{aligned} e^{S_N[\mathbf{r}]R} &= \int_{z^0 > 0}^Z d\mathbf{r}^0 [P(\mathbf{r}^0;N) - P(\mathbf{r}^0 + \mathbf{r};N)] \\ &= \text{Erf} \left[\frac{z}{b} \sqrt{\frac{3}{2N}} \right]; \end{aligned} \quad (\text{A2})$$

where $\text{Erf}(x)$ denotes the error function defined as

$$\text{Erf}(x) = \frac{2}{\sqrt{\pi}} \int_0^x e^{-t^2} dt; \quad (\text{A3})$$

We recall that the Kuhn length is related to the persistence length as $b = 2l_p$ and that for single stranded DNA $l_p \approx 5$ bp.

We sum next over all possible tail lengths. Before hybridization the target molecules are fragmented at random locations, with an average fragment length of about 50 bp. We find thus:

$$e^{S(m)R} = \left(\frac{1}{2} \right)^{m_0} \int_{N=0}^{\infty} \frac{N!}{N!} \text{Erf} \left[\frac{m + m_0}{10} \sqrt{\frac{3}{2N}} \right]; \quad (\text{A4})$$

in which $\frac{1}{2} = 49/50$ is the probability for chain continuation, and m_0 is the ratio of the spacer distance and the length of a single base pair.

-
- [1] B. Alberts et al., *Molecular Biology of the Cell* (Garland Science, New York, 2002).
- [2] R. J. Lipshutz et al., *Nature* 21, 20 (1999).
- [3] F. Naef and M. O. Magnasco, *Phys. Rev. E* 68, 011906 (2003).
- [4] V. A. Bloomfield, D. M. Crothers, and I. Tinoco, Jr., *Nucleic Acids Structures, Properties and Functions* (University Science Books, Mill Valley, 2000).
- [5] N. Sugimoto et al., *Biochemistry* 34, 11211 (1995).
- [6] R. Levicky and A. Hogan, *Trends Biotechnol.* 23, 143 (2005).
- [7] Y. Okahata et al., *Anal. Chem.* 70, 1288 (1998).
- [8] B. P. Nelson et al., *Anal. Chem.* 73, 1 (2001).
- [9] A. W. Peterson, L. K. Wolf, and R. M. Georgiadis, *J. Am. Chem. Soc.* 124, 14601 (2002).
- [10] A. Vainrub and B. M. Pettitt, *Phys. Rev. E* 66, 041905 (2002).
- [11] J. M. Deutsch and S. Liang and O. Narayan, "Modeling of microarray data with zippering", preprint q-bio.BM/0406039.
- [12] G. A. Held, G. Grinstein, and Y. Tu, *Proc. Natl. Acad. Sci.* 100, 7575 (2003).
- [13] A. Halperin, A. Buhot, and E. B. Zhulina, *Biophys. J.* 86, 718 (2004).
- [14] M. F. Hagan and A. K. Chakraborty, *J. Chem. Phys.* 120, 4958 (2004).
- [15] C. J. Burden and Y. Pittelkow and S. R. Wilson, "An adsorption model of hybridization behaviour on oligonucleotide microarrays", preprint q-bio.BM/0411005.
- [16] H. Binder and S. Preibisch, *Biophys. J.* 89, 337 (2005).
- [17] E. Carlon and T. Heim, *Physica A* 362, 433 (2006).
- [18] J. Lyklema, *Fundamentals of interface and colloid science, Fundamentals*, vol. I (Academic Press, London, 1991).
- [19] www.aymetrix.com/analysis/download/center2.aspx.
- [20] E. Carlon, T. Heim, J. Klein Wolterink and G. T. Barkema, "Comment on: Solving the riddle of the bright matches: Labeling and selective binding in oligonucleotide arrays by F. Naef and M. Magnasco", *Phys. Rev. E* (in press).
- [21] J. E. Forman et al., *ACS Symposium Series* 682, 206 (1998).
- [22] H. Binder, T. Kirsten, I. L. Hofacker, P. F. Stadler, and M. Loefer, *J. Phys. Chem. B* 108, 18015 (2004).